

Biomechanical evaluation of the Total Facet Arthroplasty System[®] (TFAS[®]): loading as compared to a rigid posterior instrumentation system

Simon G. Sjøvold · Qingan Zhu · Anton Bowden ·
Chad R. Larson · Peter M. de Bakker · Marta L. Villarraga ·
Jorge A. Ochoa · David M. Rosler · Peter A. Cripton

Received: 16 October 2008/Revised: 10 January 2012/Accepted: 28 February 2012/Published online: 10 March 2012
© Springer-Verlag 2012

Abstract

Purpose To gain insight into a new technology, a novel facet arthroplasty device (TFAS) was compared to a rigid posterior fixation system (UCR). The axial and bending loads through the implants and at the bone-implant interfaces were evaluated using an ex vivo biomechanical study and matched finite element analysis. Kinematic behaviour has been reported for TFAS, but implant loads have not. Implant loads are important indicators of an implant's performance and safety. The rigid posterior fixation system is used for comparison due to the extensive information available about these systems.

Methods Unconstrained pure moments were applied to 13 L3–S1 cadaveric spine segments. Specimens were tested intact, following decompression, UCR fixation and TFAS implantation at L4–L5. UCR fixation was via standard pedicle screws and TFAS implantation was via PMMA-cemented transpedicular stems. Three-dimensional 10 Nm moments and a 600 N follower load were applied; L4–L5

disc pressures and implant loads were measured using a pressure sensor and strain gauges, respectively. A finite element model was used to calculate TFAS bone-implant interface loads.

Results UCR experienced greater implant loads in extension ($p < 0.004$) and lateral bending ($p < 0.02$). Under flexion, TFAS was subject to greater implant moments ($p < 0.04$). At the bone-implant interface, flexion resulted in the smallest TFAS (average = 0.20 Nm) but greatest UCR (1.18 Nm) moment and axial rotation resulted in the greatest TFAS (3.10 Nm) and smallest UCR (0.40 Nm) moments. Disc pressures were similar to intact for TFAS but not for UCR ($p < 0.04$).

Conclusions These results are most applicable to the immediate post-operative period prior to remodelling of the bone-implant interface since the UCR and TFAS implants are intended for different service lives (UCR—until fusion, TFAS—indeinitely). TFAS reproduced intact-like anterior column load-sharing—as measured by disc pressure. The highest bone-implant moment of 3.1 Nm was measured in TFAS and for the same loading condition the UCR interface moment was considerably lower (0.4 Nm). For other loading conditions, the differences between TFAS and UCR were smaller, with the UCR sometimes having larger values and for others the TFAS was larger. The long-term physiological meaning of these findings is unknown and demonstrates the need for a better understanding of the relationship between spinal arthroplasty devices and the host tissue as development of next generation motion-preserving posterior devices that hope to more accurately replicate the natural functions of the native tissue continues.

S. G. Sjøvold · Q. Zhu · C. R. Larson · P. M. de Bakker ·
P. A. Cripton
Department of Orthopaedics, University of British Columbia
and Vancouver Coastal Health Research Institute,
Vancouver, BC, Canada

S. G. Sjøvold · P. M. de Bakker · P. A. Cripton (✉)
Department of Mechanical Engineering,
University of British Columbia and Vancouver Coastal Health
Research Institute, 6250 Applied Science Lane,
Vancouver, BC V6T 1Z 4, Canada
e-mail: cripton@mech.ubc.ca

A. Bowden · M. L. Villarraga
Exponent Inc., Philadelphia, PA, USA

J. A. Ochoa · D. M. Rosler
Archus Orthopedics Inc., Redmond, WA, USA

Keywords Total facet arthroplasty · Implant loading ·
Bone-implant interface · Load sharing · Lumbar spine

Introduction

Several motion-preserving spinal implants are presently in clinical use or under development including total disc replacements (TDR), synthetic nucleus replacements, flexible posterior instrumentation systems and devices that replace the facet joints [1–3]. These devices are intended to reduce the mechanisms of segmental degeneration that occur adjacent to fusion [4–6] by re-establishing the natural spinal kinematics and load-sharing at the operated segment [6–11]. Another alternative to fusion-based treatment [12] that allows resection of facet arthrosis will become available through facet joint arthroplasty systems [1, 13, 14] allowing resection of some or all of the facet joint and associated lamina. A total facet joint arthroplasty device that functionally models the intact anatomy is the Total Facet Arthroplasty System® [TFAS®; Archus Orthopedics (now defunct), Redmond, WA, USA, Fig. 1].

Pre-clinical testing is thought to have great relevance to certain aspects of the eventual clinical performance of spinal implant systems [15]. Motion-preserving spine implants have been evaluated under ex vivo human cadaver experiments [7–9, 13, 14, 16], using in vivo animal models [8] and using theoretical finite element (FE) analyses [10, 11, 17, 18]. They have also undergone in vivo wear testing studies to evaluate

the effects of wear particles in clinical service [19, 20]. As a subset of motion-preserving implants, facet replacement systems have only recently been developed, and considerably less preclinical research has been conducted for these devices [13, 14, 21]. To our knowledge, there have not been any in vivo animal models, wear or bone-implant interface strength studies reported for these systems.

One important consideration for these devices is the evaluation of the mechanical loads that are expected at the bone-implant interfaces through an ex vivo human cadaver experimental study, theoretical computation or even in vivo methods. It is important that such an evaluation be carried out to establish the postoperative safety of the device against loosening or mechanical failure. A prior study suggests that the facet loads in the natural lumbar spine could reach as high as 25 and 47 % of the total intervertebral joint load in the neutral posture for healthy and degenerated facets, respectively [22]. The natural facets also experience higher loads in torsion than in other directions under three-dimensional ex vivo flexibility testing [23]. No specific standards exist to delineate appropriate or allowable implant loads for motion-preserving facet arthroplasty devices, but significant ex vivo and in vivo clinical data of this type is available for similarly situated posterior fixation systems. Our objective was to

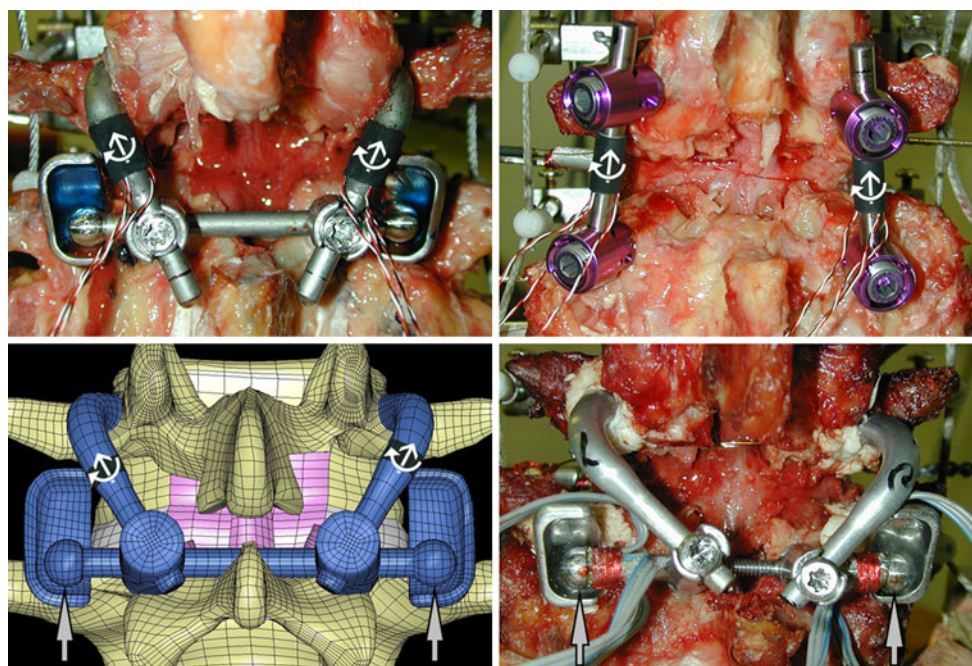


Fig. 1 Posterior view of the three experimental and finite element (FE) models used in the determination of the Total Facet Arthroplasty System (TFAS) and posterior fixation system (UCR) implant and bone-implant interface loads. Implant loads (white arrows) were derived from three strain gauges applied to the cephalad stems of the TFAS (top left) and longitudinal rods of the UCR (top right). Strain gauges applied adjacent to the cephalad bearing of the TFAS (lower

right) allowed the measurement of bearing contact loads (grey arrows). A FE model of the TFAS (lower left) was validated to the experimentally derived TFAS implant and bearing contact loads. Bone-implant interface loads were extrapolated from the implant loads of the UCR and compared to those calculated from the FE-TFAS model

characterize and compare the loads within the implant, the bone-implant interface loads and disc pressures following TFAS implantation to those of a rigid posterior fixation system using combined ex vivo and FE analyses.

Materials and methods

Specimen preparation and biomechanical loading

Six human cadaveric lumbosacral spine specimens, L3–S1, were subjected to three-dimensional flexibility testing in axial rotation, lateral bending and flexion–extension, using an unconstrained testing machine [24]. The data from an additional seven specimens were used in conjunction for the validation of the FE model. We have previously reported on the kinematic methods and results for all thirteen specimens [14]. Specimen attributes are listed in Table 1. The six donors ranged from 41 to 64 years with an average age of 49.5 years, consisting of 6 males. Each specimen was prepared by excising the musculature while preserving the osteoligamentous structure and mounting the L3 and S1 vertebrae in dental cement with the L4–L5 disc space orientated horizontally. Prior to testing each spine was screened for ligamentous integrity, pathological segmental degeneration or other pathologies that would exempt the specimens from inclusion in a clinical study.

Specimens were evaluated in four conditions: intact, injury, rigid fixation with a posterior fixation system (UCR, Seaspine, Vista, CA, USA) and following stabilization with the TFAS at the L4–L5 spinal segment. The injury model consisted of a wide decompressive laminectomy including bilateral facetectomy involving resection of the entire L4 and L5 facet joints, the L4 lamina and the L4 spinous

process [14]. The UCR utilized 5.5 mm bilateral pedicle screws coupled with longitudinal rods (Fig. 1), which were removed preceding the TFAS evaluation.

The TFAS was implanted at the injury level as per the manufacturer's surgical protocol (Fig. 1). Each pedicle hole was drilled to the appropriate length and diameter (cephalad or caudal) and polymethylmethacrylate (PMMA) bone cement was used to fix the cephalad and caudal stems. The caudal bearings were attached directly to the caudal stems and a cross-arm supporting the cephalad bearings was locked into place spanning both cephalad stems.

The spine motion simulator applied pure non-constraining ± 10 Nm moments to the top vertebra at approximately $2^\circ/\text{s}$ in flexion–extension, lateral bending, and axial rotation for three cycles [24]. A 600 N compressive preload followed the contour of the spine ensuring compression perpendicular to the endplates between each segment [25, 26]. The L4–L5 intervertebral disc pressure was monitored with a 2.1 mm diameter custom needle pressure transducer for the six specimens used to determine the implant and interface loads (Robert A. Denton, Inc., Rochester Hills, MI, USA) [27–29].

Implant measurements

TFAS and UCR implant loads (six specimens) were calculated from three uniaxial strain gauges (CEA-06-015UW-120, Vishay Intertechnology Inc., Malvern, PA, USA) aligned with the longitudinal axes of the TFAS cephalad stems and UCR rods (Fig. 1). The gauges were affixed, using epoxy adhesive, at 120° intervals around the circumference of the components. Using strain values from the independent gauges, the axial force and bending moment were calculated from theoretical beam–column stress–strain relationships at the location of the gauges [30].

Table 1 Specimen information

Specimen	Gender	Age	Race	Height (cm)	Weight (kg)
TFAS-UCR comparison and validation specimens					
H1126	M	41	Caucasian	188	100
H1127	M	64	Caucasian	173	75
H1128	M	47	Caucasian	180	82
H1134	M	40	Caucasian	180	100
H1135	M	50	Caucasian	188	122
H1138	M	55	Unknown	188	95
Validation specimens					
H1066	F	84	Unknown	182.8	95.7
H1102	F	69	Unknown	Unknown	Unknown
H1104	Unknown	Unknown	Unknown	Unknown	Unknown
H1105	Unknown	Unknown	Unknown	Unknown	Unknown
H1116	F	84	Unknown	Unknown	Unknown
H1124	Unknown	Unknown	Unknown	Unknown	Unknown
H1125	Unknown	Unknown	Unknown	Unknown	Unknown

Three uniaxial strain gauges (FLG-02-17, TML Tokyo Sokki Kenkyujo Co., Shinagawa-Ku, Tokyo) were applied to the other seven TFAS specimens, not included in the UCR subset, for the measurement of TFAS bearing contact loads (Fig. 1). Bearing contact loads were calculated by combining the axial force and bending moment into a single force vector perpendicular to the bearing surface.

Each implant was calibrated prior to testing with a material testing machine. Compressive loads (90 N) were applied collinear with the implant axis (axial force calibration) and at radial increments around the circumference of the implant (bending moment calibration). The outputs of the gauges were balanced by applying scaling factors to two of the gauges (bending moment correction) and an overall correction factor (axial force correction) was determined so that the theoretical results from the beam-column theory optimally matched the experimental results. To validate the calibration, the spine motion simulator applied multiple pure-moment (± 3.5 Nm) cycles to the end of the implant. Using these procedures, the maximum error in calculating a peak axial (90 N) or bending moment (3.5 Nm) was at most 7 and 13 %, respectively.

FE model

The cross-arm component of the TFAS rendered it statically indeterminate for the purpose of calculating bone-

implant interface loads. For this reason, a FE model was developed, validated against the current experimental data, and used to calculate the bone-implant interface loads. The detailed, nonlinear FE model of a representative lumbar (L4–L5) functional spinal unit (FSU) was generated based on commercially available surface models of the spine (Digimation, St. Rose, LA, USA). Details on the element types and material properties for each of the components of the model are presented in Table 2 [31–38]. Bone elements were assigned an isotropic, homogeneous, linear elastic material constitutive model based on applicable experimental results [36]. The annulus fibrosis was modelled as an orthotropic elastic material [33]. The nucleus was modelled as an incompressible fluid material that comprised 50 % of the total disc volume [39, 40]. The interfaces between the intervertebral discs and the endplates were continuous (node matched, displacement compatible). A tension-only, linear elastic fabric material representation was used to model the material behaviour of the seven major lumbar spine ligaments (Table 2) [39, 40].

The intact model was modified to include the TFAS in a post-implant configuration (including bilateral facetectomy). Facet contact (intact model) and arthroplasty bearing contact (implanted model) were represented using surface-to-surface penalty algorithms (LSTC 2003). The nonlinear multi-physics code LS-DYNA (Livermore Software Technology Corp., Livermore, CA, USA) was chosen

Table 2 Element types and material properties for each of the FE model components

Component/material	Element formulation	Constitutive model	Modulus (MPa)	Poisson's ratio	Cross-sectional area (mm ²)	References
Bone cement	Hexahedral	Elastic	2,340	0.20		[35]
Ti ₆ Al ₄ V	Hexahedral	Elastic	114,000	0.33		[31]
CoCrMo	Hexahedral	Elastic	220,000	0.30		[32]
Cortical bone	Shell	Elastic	12,000	0.30		[34, 37]
Posterior elements	Hexahedral	Elastic	3,500	0.25		[34, 37]
Cancellous bone	Hexahedral	Elastic	300	0.20		[36]
Endplates	Shell	Elastic	1,000	0.20		[38]
Cartilage	Shell	Elastic	10	0.40		[37]
Intervertebral disc						
Nucleus pulposus	Hexahedral	Fluid	1,667	Incompressible		[34, 37]
Inner annulus fibrosis	Hexahedral	Orthotropic Elastic	17.5/0.19/0.27	0.88/1.86/0.14		[33]
Outer annulus fibrosus	Hexahedral	Orthotropic Elastic	5.6/0.19/0.34	0.33/1.77/0.14		[33]
Ligaments						
Anterior Longitudinal	Tension-only Shell	Elastic	20	0.30	38.0	[37]
Posterior longitudinal	Tension-only Shell	Elastic	70	0.30	20.0	[37]
Ligamentum flavum	Tension-only Shell	Elastic	50	0.30	60.0	[37]
Intertransverse	Tension-only Shell	Elastic	50	0.30	10.0	[37]
Interspinous	Tension-only Shell	Elastic	28	0.30	35.5	[37]
Supraspinous	Tension-only Shell	Elastic	28	0.30	35.5	[37]
Capsular	Tension-only Shell	Elastic	20	0.30	40.0	[37]

as a software platform due to its large library of material property representations as well as its ability to adequately handle both large displacement and a variety of contact conditions. The intact model had 58,001 nodes, 52,256 hexahedral elements, and 4,918 quadrilateral shell elements. The TFAS model had 63,559 nodes, 56,260 hexahedral elements, and 4,266 quadrilateral shell elements.

FEA validation

The FEA validation was composed of two distinct phases. In the first phase, isolated TFAS cephalad components were modelled and validated against experimentally loaded cephalad components. In the second phase, the TFAS model was incorporated into the L4–L5 FSU model and validated for implant loads under displacement-controlled flexion, extension, axial rotation, and lateral bending that matched the experimentally obtained data. The displacements applied to the models were prescribed to match the helical axis and range-of-motion data for each loading mode obtained experimentally [14].

Bone-implant interface load calculation

Direct calculation of UCR bone-implant interface loads

Loading through the UCR was assumed to be primarily characterized by an axial force and pure bending moment through each independent side of the implant. This allowed the calculation of the bone-implant interface forces (bending moment and transverse shear force) from the loads measured at the strain gauge locations [27].

FE calculation of TFAS bone-implant interface loads

The TFAS FE model was exercised using load-controlled boundary conditions. A 600 N follower load was applied to the superior endplate of L4, with a 10 Nm moment to induce flexion, extension, lateral bending, or axial rotation. Transverse shear forces and bending moments at the bone-implant insertion point were extracted from the FE results at a cutplane parallel to the bone-implant interface.

Statistics

Matched pairs Student's *t* tests were used to analyze the differences between experimental implant axial forces and bending moments in the TFAS and UCR. A repeated measures analysis of variance (MANOVA) was used to evaluate the disc pressure results. Comparisons between the specific conditions were made using the Student–Newman–Keuls (SNK) post hoc test. For all tests, a 95 % level of significance was used. The statistical package

Statistica 5.1 (Statsoft, Tulsa, OK) was used for statistical analyses.

Results

The implant bending moments (Fig. 2; Table 3), implant axial forces (Fig. 2; Table 3), and bearing contact loads (Table 4) extracted to validate the finite element model generally fell within the range ($AVG \pm SD$) of the experimental TFAS data. The results of the validation experiments and FE modelling of the isolated TFAS cephalad construct yielded excellent experimental-FE agreement (data not provided).

The TFAS and UCR implant bending moments, axial forces and transverse shear loads were evaluated at the extremes of motion. The bending moments and axial forces (Fig. 2; Table 3) generally increased with the applied moment (Fig. 3). Figure 2 presents a comprehensive view of the results in all loading modes, displayed around the circumference of the radial plot. Magnitudes for the experimental work are averages only. The TFAS experienced three times greater moments than the UCR in flexion ($p < 0.04$), smaller moments on the side of loading in lateral bending ($p < 0.02$) and considerably lower moments in extension ($p < 0.004$). The axial forces (Fig. 2; Table 3) were similar for both devices in flexion, approximately three times greater in the UCR in extension ($p < 0.02$), and smaller in the TFAS on the side of loading in lateral bending ($p < 0.009$).

The TFAS FE model and UCR experienced maximum and minimum bone-implant interface bending moments in opposite loading directions (Fig. 4; Table 5). Flexion resulted in the smallest moment for the TFAS (0.20 Nm), but the greatest moment for the UCR (1.18 Nm). In contrast, axial rotation resulted in the greatest TFAS moment (3.10 Nm) and the smallest UCR moment (0.40 Nm). In axial rotation, only the contralateral side of the TFAS to the direction of rotation experienced a greater moment (more than three times) than the UCR. The moments on the ipsilateral side of both implants were of similar magnitude. The cephalad arm of the TFAS experiencing the greatest bending moment varied with the direction of motion in lateral bending. In contrast, the UCR moment was always largest at the same pedicle for both left and right lateral bending, although the pedicle experiencing the greatest bending moment varied from right to left for different installations. The moments in the left and right sides of the TFAS and UCR were symmetric in flexion and extension, but the magnitudes were greater at the TFAS interface in extension and at the UCR interface in flexion.

The bone-implant interface transverse shear loads were always oriented superiorly for the TFAS regardless of the

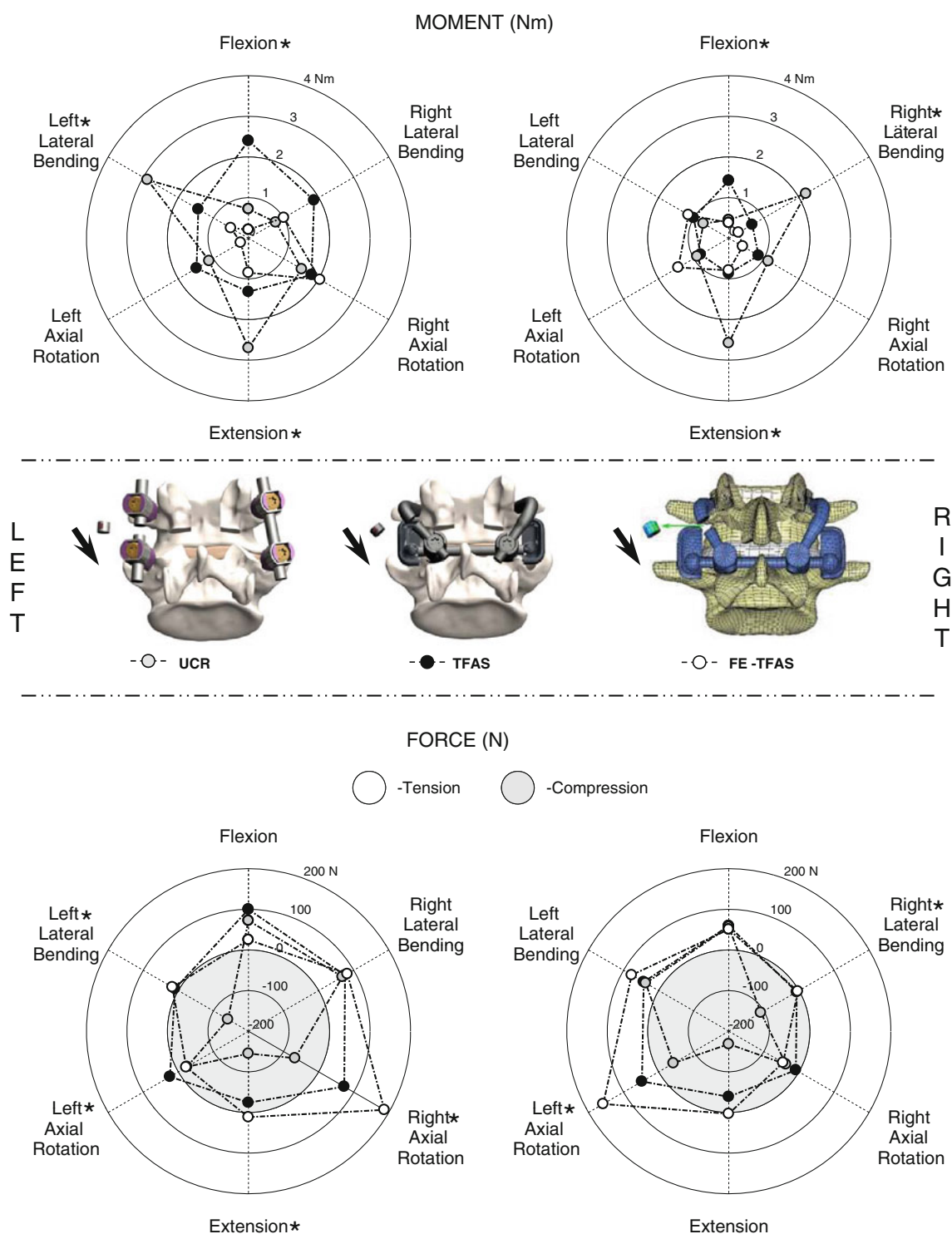


Fig. 2 The left and right implant bending moments (*top*) and axial forces (*bottom*) derived experimentally (average only) from the Total Facet Arthroplasty System (TFAS; $n = 6$) and posterior fixation system (UCR; $n = 6$). Similar loads were determined from a finite element model (FE-TFAS) of the TFAS. The axial force plots are separated into tensile (positive; white) and compressive (negative;

gray) regions. The representative images in the centre illustrate the regions from which the loads were derived for each model. Significant differences ($p < 0.05$) between TFAS and UCR are indicated by asterisk next to the label for the direction of loading (e.g. bending moment flexion). Means and standard deviations for this data series can be found in Table 3

Table 3 Implant bending moment and axial force derived experimentally from TFAS ($n = 6$) and UCR ($n = 6$) implants and theoretically from FE-TFAS model

Loading mode	Implant side	Implant bending moments (Nm)			Implant axial force (N)		
		TFAS	UCR	FE-TFAS	TFAS	UCR	FE-TFAS
Flexion	Left						
	Mean	2.40*	0.72	0.21	99.8	72.3	25.1
	SD	1.46	0.25	–	66.1	35.8	–
	Right						
	Mean	1.42*	0.45*	0.38	59.2	57.3	50.8
Extension	Left						
	Mean	1.32*	2.70*	0.85	–24.1*	–145.0*	11.6
	SD	1.05	0.69	–	–23.4	–71.8	–
	Right						
	Mean	0.87*	2.58*	0.79	–38.6	–168.3	3.2
Left axial rotation	Left						
	Mean	1.48	1.12	0.22	23.9*	–24.8*	–22.5
	SD	0.99	0.81	–	49.0	–55.6	–
	Right						
	Mean	0.80	0.90	1.44	47.56*	–42.3*	157.9
Right axial rotation	Left						
	Mean	1.80	1.52	2.04	73.1*	–67.1*	187.4
	SD	1.15	0.51	–	44.4	–36.7	–
	Right						
	Mean	0.85	1.13	0.40	–8.9	–37.1	–45.2
Left lateral bending	Left						
	Mean	1.43*	2.88*	0.50	9.5*	–141.6*	16.8
	SD	1.07	0.94	–	41.8	–66.4	–
	Right						
	Mean	1.00	0.72	1.15	42.6	36.7	76.6
Right lateral bending	Left						
	Mean	1.87	0.78	1.01	75.3	68.0	82.1
	SD	1.34	0.6	–	68.2	59.2	–
	Right						
	Mean	0.67*	2.20*	0.28	–6.3*	–108.7*	–3.2

TFAS Total Facet Arthroplasty System, UCR posterior fusion system, FE finite element, SD standard deviation

* Significant difference between TFAS and UCR

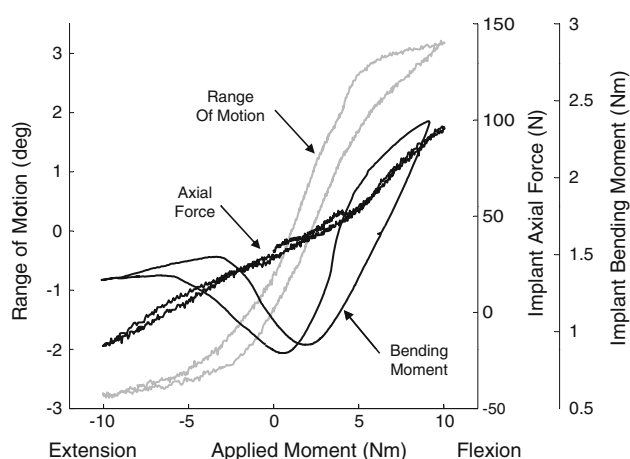
direction of loading, while the UCR varied in orientation superiorly and inferiorly (Fig. 4; Table 5). The TFAS and UCR shear loads were symmetric and similar in magnitude in flexion (TFAS: 78 and 73 N, UCR: 72 and 57 N), but greater and orientated inferiorly in the UCR in extension (UCR: –145 and –168 N; TFAS: 78 and 82 N). The greatest TFAS and UCR shear loads were seen in axial

rotation (TFAS: 172 and 101 N; UCR: –67 and –42 N) at the interface opposite to the direction of rotation. The orientation of loading was inferior for both sides of the UCR in comparison to the TFAS. The TFAS shear was symmetric in lateral bending with smaller loads (range 45–60 N) in comparison to other loading directions. In comparison, the ipsilateral side of the UCR to the direction

Table 4 Cephalad bearing contact force derived experimentally from TFAS ($n = 7$) implant and theoretically from FE-TFAS model

Motion	Implant side	TFAS contact force \pm SD (N)	FE-TFAS contact force (N)
Flexion	Left	81.4 \pm 18.6	37.0
	Right	78.3 \pm 48.1	41.0
Extension	Left	99.0 \pm 47.2	84.1
	Right	85.2 \pm 75.6	92.6
Axial rotation—left	Left	26.7 \pm 19.2	0.0
	Right	63.4 \pm 36.8	186.7
Axial rotation—right	Left	72.0 \pm 10.1	193.6
	Right	31.1 \pm 42.9	0.0
Lateral bending—left	Left	34.7 \pm 15.0	69.8
	Right	42.9 \pm 36.4	52.2
Lateral bending—right	Left	59.1 \pm 44.7	43.5
	Right	28.9 \pm 27.4	76.1

TFAS Total Facet Arthroplasty System, FE finite element, SD standard deviation

**Fig. 3** Typical moment versus Total Facet Arthroplasty System (TFAS) range of motion (ROM), TFAS axial force and TFAS bending moment of the L4–L5 segment in flexion–extension

of lateral bending experienced greater shears loads (−142 and −109 N).

In general the intact L4–L5 intervertebral disc pressure was consistent with pressure patterns of healthy lumbar intervertebral discs, increasing in flexion and extension from the neutral position (Fig. 5). In comparison to intact, the UCR neutral position disc pressure was significantly less in axial rotation ($p < 0.04$) and lateral bending ($p < 0.025$). The maximum pressure also decreased significantly at peak extension ($p < 0.04$) for the UCR. The TFAS was similar to the intact spine throughout the flexion–extension, lateral bending and axial rotation range of motions.

Discussion

Novel spine implants, such as the TFAS, must undergo extensive preclinical testing such as wear, biocompatibility,

strength, load-sharing, fatigue and kinematic testing [15]. These tests are performed to provide a limited indication of the expected clinical performance of the implant. We have previously reported on the kinematic behaviour of this implant [14]. In the current study, we calculated the loads at the TFAS bone-implant interfaces, a key parameter that indicates the potential for bone-implant fracture or interface loosening. There are no guidelines to identify allowable stresses from a facet arthroplasty device, and for this reason, we evaluated the TFAS loads in the context of a posterior fixation system derived from a device family that has amassed considerable clinical experience.

Our a priori expectation was that the TFAS, by virtue of its motion-sparing design, would experience different and likely smaller implant and bone-implant interface loads than the rigid UCR. However, our results are inconclusive on this point: statistically speaking the experimental data shows that within the implants TFAS bending moments were greater than UCR moments for flexion but less than UCR moments for extension. UCR experienced higher moments than TFAS in ipsilateral lateral bending and there were not significant differences in contralateral bending or in either direction of torsion. Similar mixed loading mode-dependent differences existed for the other load metrics. The TFAS stress levels as estimated by the FE model, are well within the static and fatigue strengths of the implant's material and this has also been previously confirmed on the benchtop [41].

The differences in implant and bone-implant interface loads were likely due to the distinct load-sharing behaviour and design philosophies between the two implants. Clinical and ex vivo experience has demonstrated that pedicle screw systems provide the least constraint to loading in axial rotation but are relatively rigid in all other loading directions [14, 27]. Therefore, it is not surprising that the UCR experienced the highest implant loads under lateral bending and extension. Flexion would appear to be an

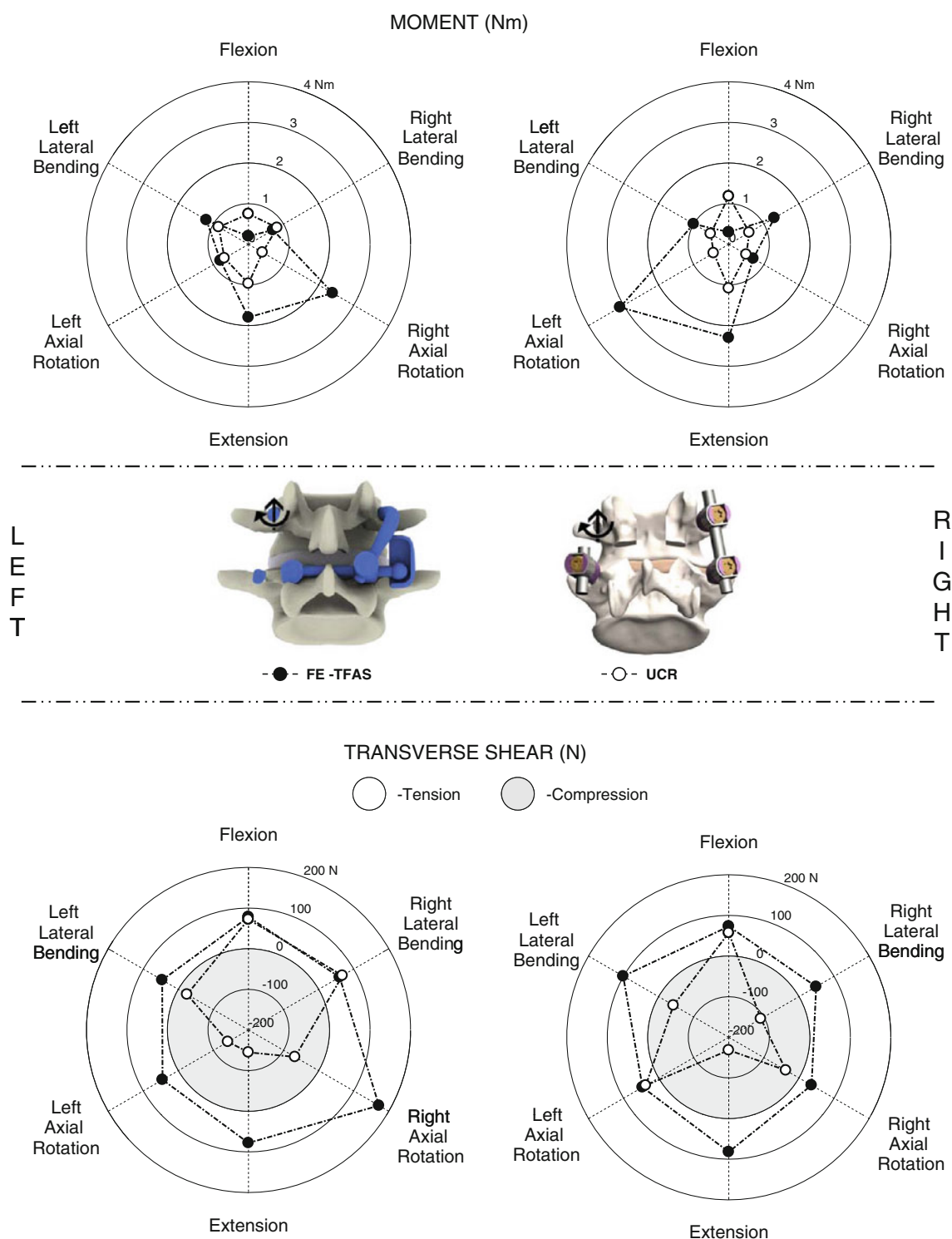


Fig. 4 The left and right bone-implant interface bending moments (top) and transverse shear loads (bottom) derived experimentally from the posterior fixation system (UCR: $n = 6$) and theoretically from a finite element model of the Total Facet Arthroplasty System (FE-TFAS). The transverse shear plots are separated into inferiorly

(positive; white) and superiorly (negative; gray) directed regions. The representative images in the centre illustrate the plane at the bone-implant interface from which the loads were derived for each model. Means and standard deviations for this data series can be found in Table 5

Table 5 Bone-implant bending moment and transverse shear force derived experimentally from UCR ($n = 6$) implants and theoretically from FE-TFAS model

Loading mode	Implant side	Bone-implant interface bending moments (Nm)		Bone-implant interface transverse shear (N)	
		FE-TFAS	UCR	FE-TFAS	UCR
Flexion	Left				
	Mean	0.20	0.75	78.0	72.3
	SD	–	0.59	–	35.7
	Right				
	Mean	0.30	1.18	73.0	57.3
Extension	Left				
	Mean	1.80	0.97	78.0	–145.0
	SD	–	0.73	–	–71.8
	Right				
	Mean	2.30	1.08	82.0	–168.3
Left axial rotation	Left				
	Mean	0.80	0.68	46.0	–24.8
	SD	–	0.37	–	–55.6
	Right				
	Mean	3.10	0.43	101.0	–42.3
Right axial rotation	Left				
	Mean	2.40	0.40	172.0	–67.1
	SD	–	0.40	–	–36.7
	Right				
	Mean	0.70	0.50	36.0	–37.1
Left lateral bending	Left				
	Mean	1.20	0.85	45.0	–141.6
	SD	–	0.68	–	–66.4
	Right				
	Mean	1.00	0.52	46.0	36.7
Right lateral bending	Left				
	Mean	0.70	0.82	60.0	68.0
	SD	–	0.58	–	59.2
	Right				
	Mean	1.30	0.58	49.0	–108.7
	Left				
	Mean	0.70	0.82	60.0	68.0
	SD	–	0.58	–	59.2
	Right				
	Mean	1.30	0.58	49.0	–108.7

TFAS Total Facet Arthroplasty System, UCR posterior fusion system, FE finite element, SD standard deviation

exception to the above “rule of thumb” because TFAS had higher implant loads than UCR in flexion. The UCR may have had lower bending moments than the TFAS in flexion because the stabilized spine supported the applied moment through a force couple involving the intervertebral disc and the posterior instrumentation system [27]. Or, the TFAS may have measured higher bending moments than the UCR system under flexion because the specific coupling between

anterior translation and flexion rotation in the lumbar spine altered the load vector generated at the cephalad bearing surface resulting in a larger moment arm relative to the measurement point on the TFAS arm than was the case for extension or lateral bending. In contrast, the TFAS constrains motions, when the TFAS articulations approach the end of their motion, via a more robust mechanism compared to the UCR (i.e. direct surface to surface articulation

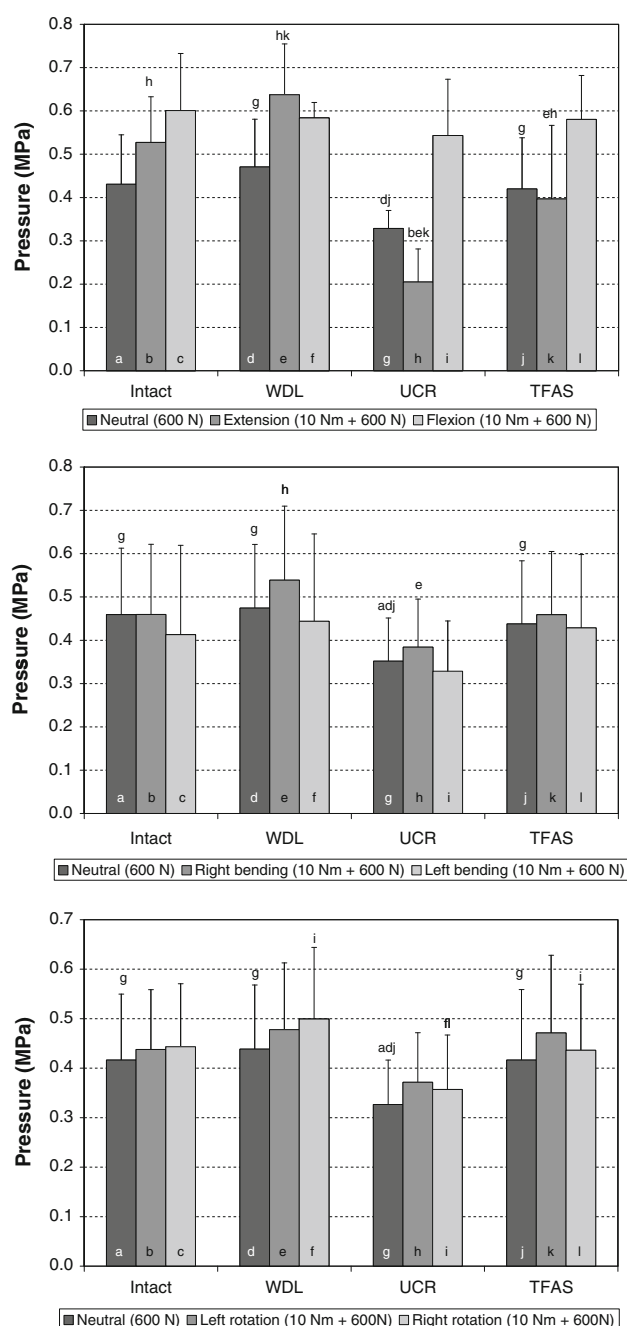


Fig. 5 Average disc pressures in the intact spine ($n = 6$), following a wide decompressive laminectomy (WDL: $n = 6$) and implantation of the Total Facet Arthroplasty System (TFAS: $n = 6$) and posterior fixation system (UCR: $n = 6$) of the L4–L5 segment in flexion–extension (*top*), lateral bending (*middle*) and axial rotation (*bottom*). The error bars represent one standard deviation. Significant differences ($p < 0.05$) are indicated at the top of each bar (i.e. ‘hk’ at the top of bar ‘e’ indicates that the bar is statistically different from bar ‘h’ and ‘k’ as indicated at the base of the graph)

in the TFAS versus bending or torsion of the UCR longitudinal rods). The TFAS mechanism was specifically designed to simulate the loading of the natural facets. This attempt to recreate natural facet joint mechanics—natural

lumbar facets experience high loads in axial rotation relative to the other directions—[23, 42] is probably the cause of the large TFAS versus UCR implant–bone interface load differences under axial torsion.

The implantation angle (relative to the sagittal plane) of the two implant system was different. The UCR rods were generally aligned with the sagittal plane whereas the TFAS Cephalad arms were angled between 17 and 40° from the sagittal plane. The dissimilarity in implantation angle of the strain-gauge instrumented component of the two implant systems is a limitation of this study and may have contributed to the differences in the implant and bone–implant interface loads. However, we examined the relationship between implant angle and implant load for both TFAS and UCR (which also varied slightly from vertical). No direct relationship between implant angle and implant load could be discerned for either implant. This indicates that the difference in the implant loads estimated for UCR and TFAS that was due to the angle of the implant was likely minimal in comparison to the differences due to design philosophy and anatomic variation.

One of the goals of many motion-preserving devices is to reproduce intact tissue load sharing, while fusion systems such as the UCR do not typically attempt to maintain specific tissue loading patterns. TFAS is designed to restore the posterior stability and motion of stenotic patients post-decompression and is meant to complement the existing anterior column elements in a manner similar to the natural facets [14]. TFAS is currently contraindicated for cases of anterior column pathology or injury that results in substantial listhesis. The intervertebral disc pressure provides a measure of anterior column load sharing. For TFAS, the L4/L5 intradiscal pressure was similar to the intact segments in all directions of motion, but the same was not true for the UCR.

To our knowledge, this is the first study of implant and bone–implant interface loads pertaining to a facet arthroplasty device, an important component of the pre-clinical evaluation of these novel clinical devices. The data pertains directly to the risk of implant failure (implant loads) or bone–implant interface loosening (bone–implant loads) in the clinical situation. The highest implant moment of 2.88 Nm was measured in the UCR during lateral bending and the TFAS experience the greatest implant moment in flexion (2.40 Nm). These magnitudes are similar to the implant loads recorded in previous pure-moment biomechanical studies of posterior fixation systems [27, 43]. They are also similar to the in vivo loads measured in spine fixation implants during everyday activities such as standing, walking, bending and lying down [44–46]. At the bone–implant interface, the TFAS experienced the highest overall bending moment of 3.10 Nm during axial rotation and the UCR experience the greatest bone–implant moment

under flexion loading (1.18 Nm). This may indicate that the TFAS is at risk of higher bone-implant loosening than the UCR under axial rotation. However, the precise bending moments resulting in bone growth or resorption at the bone-implant interface are unknown and the use of PMMA to augment the fixation of the TFAS prevents us from establishing whether the risk for implant loosening would be greater for the TFAS.

The TFAS is designed for bone fixation with PMMA bone cement. PMMA augmentation is known to increase the fixation strength of pedicle screws [47–49], but unlike pedicle screws, the textured TFAS stems are unthreaded so a direct correlation may not be relevant. However, in previous in house testing at Archus Orthopedics, the fixation strength of the cemented TFAS was found to be more than twice that of the fixation strength of a similar configuration of standard pedicle screws in bone [41].

The accuracy of the TFAS FE model can be estimated from the implant validation study, where a strong agreement was found between both the experimental and FE results. The experimental results exhibited considerable variation as is expected for biologic specimens, and this contributed to some of the variability with the FE model. A substantial deviation of the FE moment from the experimental results was observed under flexion in which the FE model predicted a much smaller moment magnitude. Potential sources for this discrepancy include numerical issues (inadequacies in contact conditions), variation in placement and angle (surgical versus numerical) of the TFAS device, and choice of strain gauge (uniaxial versus rosette), and strain gauge placement variability between the experimental and FE studies.

It is important to note that the current experiments were conducted under spinal loading that is an idealized laboratory representation of the expected loads in vivo. Actual in vivo loads are known to be both more complex and of higher magnitude than the loads applied in this protocol [50–53]. Nevertheless, the current work is consistent with standard practice for conducting these evaluations and the spine research community is accustomed to interpreting in vivo clinical performance from ex vivo laboratory tests such as these. A further strength of this study was the use of a follower load to simulate the effect of torso musculature and of the weight of the body above the segment. This likely increased the loads at the implant bone interface and provided a more realistic mechanical basis for the comparison of the two implant systems.

In this study we have implicitly used the UCR as an indication of appropriate implant loads. The UCR, as a representative posterior instrumentation system with considerable documented clinical experience, is similar to the TFAS in terms of placement and by virtue of its transpedicular fixation. These results are most applicable to

the immediate post-operative period in patients since the TFAS and UCR are intended to have different service lives (UCR until fusion, TFAS indefinitely) and the complex biological interactions that occur in vivo cannot be adequately represented by current state of the art experimental or FE modelling. However, extrapolation of the data to the long-term performance of the TFAS is not possible since the interactions and effects of bone remodelling cannot be simulated ex vivo. The TFAS consistently reproduced disc pressures that were similar to the intact segment throughout all ranges of motion suggesting good reproduction of intact-like load sharing in this implant. The TFAS implant load magnitudes were similar to those reported previously for posterior fixation systems ex vivo and following implantation in patients. The highest bone-implant moment of 3.1 Nm was measured in TFAS and for the same loading condition the UCR bone-implant interface only experienced 0.4 Nm. This result is not unexpected as the TFAS was designed to replicate the shape of the natural facets and these have also been shown to experience higher loads in torsion than in other directions during ex vivo loading. Further research is warranted to determine the physiological meaning of these findings as the relationship between the bone-implant interface loads of these magnitudes in the spine and the long-term efficacy of the implant is not known. This study demonstrates the need for a better understanding of the relationship between spinal arthroplasty devices and the host tissue as development of next generation devices that hope to more accurately replicate the natural functions of the native tissue continues.

Acknowledgments Financial support in the form of a research grant from Archus Orthopedics, Redmond, Washington is gratefully acknowledged. We also thank Dr. Thomas Oxland for invaluable comments and suggestions on the manuscript.

Conflict of interest AB and MLV are employees of Exponent and JAO and DMR are employees of Archus. Exponent received consulting income from Archus. All other authors have no conflict of interest.

References

1. Acosta FL Jr, Aryan HE, Ames CP (2005) Emerging directions in motion preservation spinal surgery. *Neurosurg Clin N Am* 16(4):665–669, vii
2. Mayer HM, Korge A (2002) Non-fusion technology in degenerative lumbar spinal disorders: Facts, questions, challenges. *Eur Spine J* 11(Suppl 2):S85–S91
3. Singh K, An HS (2006) Motion preservation technologies: alternatives to spinal fusion. *Am J Orthop* 35(9):411–416
4. Ghiselli G, Wang JC, Bhatia NN, Hsu WK, Dawson EG (2004) Adjacent segment degeneration in the lumbar spine. *J Bone Joint Surg Am* 86-A(7):1497–1503

5. Hilibrand AS, Robbins M (2004) Adjacent segment degeneration and adjacent segment disease: the consequences of spinal fusion? *Spine J* 4(6 Suppl):190S–194S
6. Park P, Garton HJ, Gala VC, Hoff JT, McGillicuddy JE (2004) Adjacent segment disease after lumbar or lumbosacral fusion: review of the literature. *Spine* 29(17):1938–1944
7. Crawford NR (2005) Biomechanics of lumbar arthroplasty. *Neurosurg Clin N Am* 16(4):595–602, v
8. Cunningham BW (2004) Basic scientific considerations in total disc arthroplasty. *Spine J* 4(6 Suppl):219S–230S
9. Cunningham BW, Gordon JD, Dmitriev AE, Hu N, McAfee PC (2003) Biomechanical evaluation of total disc replacement arthroplasty: an in vitro human cadaveric model. *Spine* 28(20):S110–S117
10. Galbusera F, Fantigrossi A, Raimondi MT, Sassi M, Fornari M, Assietti R (2006) Biomechanics of the c5–c6 spinal unit before and after placement of a disc prosthesis. *Biomech Model Mechanobiol* 5(4):253–261
11. Goel VK, Grauer JN, Patel T, Biyani A, Sairyo K, Vishnubhotla S, Matyas A, Cowgill I, Shaw M, Long R, Dick D, Panjabi MM, Serhan H (2005) Effects of charite artificial disc on the implanted and adjacent spinal segments mechanics using a hybrid testing protocol. *Spine* 30(24):2755–2764
12. Atlas SJ, Delitto A (2006) Spinal stenosis: surgical versus non-surgical treatment. *Clin Orthop Relat Res* 443:198–207
13. Wilke HJ, Schmidt H, Werner K, Schmolz W, Drumm J (2006) Biomechanical evaluation of a new total posterior-element replacement system. *Spine* 31(24):2790–2796 (discussion 2797)
14. Zhu Q, Larson CR, Sjøvold SG, Rosler DM, Keynan O, Wilson DR, Cipton PA, Oxland TR (2007) Biomechanical evaluation of the total facet arthroplasty system: 3-dimensional kinematics. *Spine* 32(1):55–62
15. Goel VK, Panjabi MM, Patwardhan AG, Dooris AP, Serhan H (2006) Test protocols for evaluation of spinal implants. *J Bone Joint Surg Am* 88(Suppl 2):103–109
16. DiAngelo DJ, Foley KT, Morrow BR, Schwab JS, Song J, German JW, Blair E (2004) In vitro biomechanics of cervical disc arthroplasty with the prodisc-c total disc implant. *Neurosurg Focus* 17(3):E7
17. Denoziere G, Ku DN (2006) Biomechanical comparison between fusion of two vertebrae and implantation of an artificial intervertebral disc. *J Biomech* 39(4):766–775
18. Goel VK, Kiapour A, Faizan A, Krishna M, Friesem T (2007) Finite element study of matched paired posterior disc implant and dynamic stabilizer (360 motion preservation system). *SAS J* 01(01):55–62
19. Chang BS, Brown PR, Sieber A, Valdevit A, Tateno K, Kostuik JP (2004) Evaluation of the biological response of wear debris. *Spine J* 4(6 Suppl):239S–244S
20. Jacobs JJ, Hallab NJ, Urban RM, Wimmer MA (2006) Wear particles. *J Bone Joint Surg Am* 88(Suppl 2):99–102
21. Goel VK, Mehta A, Jangra J, Faizan A, Kiapour A, Hoy RW, Fauth AR (2007) Anatomic facet replacement system (afrs) restoration of lumbar segment mechanics to intact: a finite element study and in vitro cadaver investigation. *SAS J* 01(01):46–54
22. Yang KH, King AI (1984) Mechanism of facet load transmission as a hypothesis for low-back pain. *Spine* 9(6):557–565
23. Zhu QA, Park YB, Sjøvold SG, Niosi CA, Wilson DC, Cipton PA, Oxland TR (2008) Can extra-articular strains be used to measure facet contact forces in the lumbar spine? An in vitro biomechanical study. *Proc Inst Mech Eng [H]* 222(2):171–184
24. Goertzen DJ, Lane C, Oxland TR (2004) Neutral zone and range of motion in the spine are greater with stepwise loading than with a continuous loading protocol. An in vitro porcine investigation. *J Biomech* 37(2):257–261
25. Cipton PA, Bruehlmann SB, Orr TE, Oxland TR, Nolte LP (2000) In vitro axial preload application during spine flexibility testing: Towards reduced apparatus-related artefacts. *J Biomech* 33(12):1559–1568
26. Patwardhan AG, Havey RM, Carandang G, Simonds J, Voronov LI, Ghanayem AJ, Meade KP, Gavin TM, Paxinos O (2003) Effect of compressive follower preload on the flexion-extension response of the human lumbar spine. *J Orthop Res* 21(3):540–546
27. Cipton PA, Jain GM, Wittenberg RH, Nolte LP (2000) Load-sharing characteristics of stabilized lumbar spine segments. *Spine* 25(2):170–179
28. Frei H, Oxland TR, Nolte LP (2002) Thoracolumbar spine mechanics contrasted under compression and shear loading. *J Orthop Res* 20(6):1333–1338
29. Steffen T, Baramki HG, Rubin R, Antoniou J, Aebi M (1998) Lumbar intradiscal pressure measured in the anterior and posterolateral annular regions during asymmetrical loading. *Clin Biomech (Bristol, Avon)* 13(7):495–505
30. Perry CC (2003) Separate measurements of combined loads. http://www.vishay.com/brands/measurements_group/guide/ta/msg/msg.htm
31. Carpenter Technology Corporation (2000) Titanium Alloy Ti 6Al-4V [Technical Datasheet]. <http://cartech.ides.com/datasheet.aspx?i=101&E=269> (7/01/2000)
32. Carpenter Technology Corporation (2007) BioDur Carpenter CCM Alloy [Technical Datasheet]. <http://cartech.ides.com/datasheet.aspx?i=101&E=8> (1/18/2007)
33. Elliott DM, Setton LA (2001) Anisotropic and inhomogeneous tensile behavior of the human annulus fibrosus: experimental measurement and material model predictions. *J Biomech Eng* 123(3):256–263
34. Kumaresan S, Yoganandan N, Pintar FA, Maiman DJ (1999) Finite element modeling of the cervical spine: role of intervertebral disc under axial and eccentric loads. *Med Eng Phys* 21(10):689–700
35. Lewis G (2003) Fatigue testing and performance of acrylic bone-cement materials: state-of-the-art review. *J Biomed Mater Res B Appl Biomater* 66(1):457–486
36. Morgan EF, Bayraktar HH, Keaveny TM (2003) Trabecular bone modulus-density relationships depend on anatomic site. *J Biomech* 36(7):897–904
37. Polikeit A, Nolte LP, Ferguson SJ (2003) The effect of cement augmentation on the load transfer in an osteoporotic functional spinal unit: finite-element analysis. *Spine* 28(10):991–996
38. Silva MJ, Keaveny TM, Hayes WC (1997) Load sharing between the shell and centrum in the lumbar vertebral body. *Spine* 22(2):140–150
39. Kumaresan S, Yoganandan N, Pintar FA (1999) Finite element analysis of the cervical spine: a material property sensitivity study. *Clin Biomech (Bristol, Avon)* 14(1):41–53
40. Polikeit A, Ferguson SJ, Nolte LP, Orr TE (2003) Factors influencing stresses in the lumbar spine after the insertion of intervertebral cages: finite element analysis. *Eur Spine J* 12(4):413–420
41. Webb S (2006) Chapter 46: Total facet arthroplasty system (tfas). In: Kim DH, Cammisa FP, Fessler RG (eds) *Dynamic reconstruction of the spine*. Thieme, New York, p xix
42. Haberb H, Cipton PA, Orr TE, Beutler T, Frei H, Lanksch WR, Nolte LP (2004) Kinematic response of lumbar functional spinal units to axial torsion with and without superimposed compression and flexion/extension. *Eur Spine J* 13(6):560–566
43. Rohlmann A, Riley LH, Bergmann G, Graichen F (1996) In vitro load measurement using an instrumented spinal fixation device. *Med Eng Phys* 18(6):485–488
44. Rohlmann A, Bergmann G, Graichen F (1997) Loads on an internal spinal fixation device during walking. *J Biomech* 30(1):41–47

45. Rohlmann A, Bergmann G, Graichen F, Weber U (1997) Comparison of loads on internal spinal fixation devices measured in vitro and in vivo. *Med Eng Phys* 19(6):539–546
46. Rohlmann A, Graichen F, Weber U, Bergmann G (2000) 2000 volvo award winner in biomechanical studies: Monitoring in vivo implant loads with a telemeterized internal spinal fixation device. *Spine* 25(23):2981–2986
47. Renner SM, Lim TH, Kim WJ, Katolik L, An HS, Andersson GB (2004) Augmentation of pedicle screw fixation strength using an injectable calcium phosphate cement as a function of injection timing and method. *Spine* 29(11):E212–E216
48. Tan JS, Kwon BK, Dvorak MF, Fisher CG, Oxland TR (2004) Pedicle screw motion in the osteoporotic spine after augmentation with laminar hooks, sublaminar wires, or calcium phosphate cement: A comparative analysis. *Spine* 29(16):1723–1730
49. Wittenberg RH, Lee KS, Shea M, White AA 3rd, Hayes WC (1993) Effect of screw diameter, insertion technique, and bone cement augmentation of pedicular screw fixation strength. *Clin Orthop Relat Res* 296:278–287
50. Cholewicki J, McGill SM, Norman RW (1995) Comparison of muscle forces and joint load from an optimization and emg assisted lumbar spine model: towards development of a hybrid approach. *J Biomech* 28(3):321–331
51. Reeves NP, Cholewicki J (2003) Modeling the human lumbar spine for assessing spinal loads, stability, and risk of injury. *Crit Rev Biomed Eng* 31(1–2):73–139
52. Wilke HJ, Neef P, Caimi M, Hoogland T, Claes LE (1999) New in vivo measurements of pressures in the intervertebral disc in daily life. *Spine* 24(8):755–762
53. Wilke HJ, Rohlmann A, Neller S, Graichen F, Claes L, Bergmann G (2003) Issls prize winner: a novel approach to determine trunk muscle forces during flexion and extension: a comparison of data from an in vitro experiment and in vivo measurements. *Spine* 28(23):2585–2593